

Duplex Contextual Relation Network for Polyp Segmentation

Zijin Yin, Kongming Liang, Zhanyu Ma, and Jun Guo

Beijing University of Posts and Telecommunications, Beijing, China

<https://github.com/PRIS-CV/DCRNet>

Abstract. Polyp segmentation is of great importance in the early diagnosis and treatment of colorectal cancer. Since polyps vary in their shape, size, color, and texture, accurate polyp segmentation is very challenging. One promising way to mitigate the diversity of polyps is to model the contextual relation for each pixel such as using attention mechanism. However, previous methods only focus on learning the dependencies between the position within an individual image and ignore the contextual relation across different images. In this paper, we propose Duplex Contextual Relation Network (DCRNet) to capture both within-image and cross-image contextual relations. Specifically, we first design *Interior Contextual-Relation Module* to estimate the similarity between each position and all the positions within the same image. Then *Exterior Contextual-Relation Module* is incorporated to estimate the similarity between each position and the positions across different images. Based on the above two types of similarity, the feature at one position can be further enhanced by the contextual region embedding within and across images. To store the characteristic region embedding from all the images, a memory bank is designed and operates as a queue. Therefore, the proposed method can relate similar features even though they come from different images. We evaluate the proposed method on the EndoScene, Kvasir-SEG and the recently released large-scale PICCOLO dataset. Experimental results show that the proposed DCRNet outperforms the state-of-the-art methods in terms of the widely-used evaluation metrics.

Keywords: Computer aided diagnosis · Polyp Segmentation · Attention Mechanism · Deep learning

1 Introduction

Colorectal cancer (CRC) is the third most commonly diagnosed cancer type worldwide [20]. As the gold standard procedure for CRC screening and prevention, colonoscopy enables doctors to localize and remove the colorectal polyps which may gradually become malignant. Since this screening procedure is manual and requires expensive labor, the misdiagnosis rate is relatively high. Therefore, automatic colonoscopy methods can help clinicians accurately locate polyp areas and play a crucial role in the early diagnosis and treatment of colorectal cancer.

However, polyp segmentation is a challenging task since the polyps often vary in size, color, and texture. In addition, the boundary of polyp is usually blurred which may cause the missing detection of polyps.

Traditional polyp segmentation methods [12,21] design hand-crafted features (e.g. color, texture, shape, appearance) to distinguish a polyp from its surroundings. Due to the poor representation ability of hand-crafted features, the performance of the above methods is far from satisfactory. With the development of deep learning, numerous fully convolutional neural networks [28,31,1,2,26,10,15,18] have been applied to polyp segmentation. To utilize boundary information, SFANet [6] employs two decoder branches to detect polyp regions and boundaries respectively. In addition, many researchers exploit contextual relation modeling for image segmentation. ACSNet[30] combines the global context and local details in the decoder branch to deal with the shape and size variance of polyps regions. PraNet[5] generates a coarse segmentation map by aggregating the multi-scale features and extract silhouette according to the local features. As the most common way to model contextual relation, the self-attention mechanism [7,29] augments the representation for each pixel by capturing its multi-scale context relation. However, the above methods only consider the semantic relations within an image and ignore the representation consistency of the same semantic classes across different images. As shown in the previous works [16,8,23], cross-image relation modeling has demonstrated its superiority improvement on various tasks. In clinical application, lesion retrieval from other images is important in radiology and can help a specialist to decide on the type of lesion and treatment planning [14]. Motivated by the above thoughts, we consider modeling contextual relations, not only within an image but also cross images, and apply it to polyp segmentation.

In this paper, we propose the Duplex Contextual Relation Network (DCR-Net) to capture the contextual relations within an individual image and across images. Specifically, we design two parallel attention modules which can be incorporated into any encoder-decoder architecture (e.g U-Net[18]). The first module is called as *Interior Contextual-Relation Module* which estimates the similarity between each position and all the positions within the same image. The feature at one position is further aggregated by the features at all positions according to the estimated similarity. The second module is called as *Exterior Contextual-Relation Module* which estimates the similarity between each position and the positions across different images. Based on the across-image similarity, the feature at one position can be further enhanced by the contextual region embedding from another image through feature aggregation. To achieve this, we employ a memory bank that operates as a queue to store the characteristic region embedding from all the images. Therefore, similar features would be related to each other even though they come from different images.

In summary, our contributions are:

1. We propose a novel Duplex Contextual Relation Network (DCRNet) to capture the contextual relations within an individual image and across images.

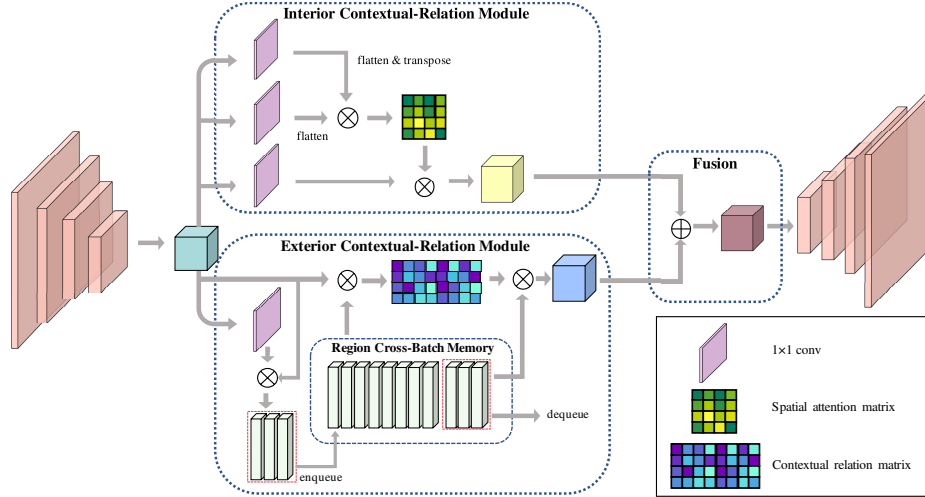


Fig. 1. An overview of the proposed DCRNet

2. A memory bank is designed and operates as a queue to store the characteristic region embedding from all the images.
3. Extensive experiments demonstrate that the proposed DCRNet outperforms the state-of-the-art methods on three public datasets.

2 Method

2.1 Overview

As illustrated in Figure. 1, we design two types of contextual relation modules to draw global contextual information over local representations generated by a backbone network. We utilize ResNet-34 as the encoder backbone. The features from the last encoder are processed by two parallel modules: Interior Contextual-Relation Module (ICR) and Exterior Contextual-Relation Module (ECR). The proposed memory bank in ECR works as a queue to store up-to-date embedding features from previous mini-batches. Finally, we fuse the features from two blocks to obtain augmented representations for pixel-level prediction.

2.2 Interior Contextual-Relation Module

As demonstrated by the Fu *et al.*[7], self-spatial-attention mechanism could adaptively integrate local features with their global dependencies. Following this idea,

we adopt Position Attention Module $s(\cdot)$ [7] to capture contextual relations between any two pixels. Specifically, given a feature $\mathbf{A} \in \mathbb{R}^{C \times H \times W}$ from encoder, the augmented region representation is computed by $\mathbf{B} = s(\mathbf{A}) \in \mathbb{R}^{C \times H \times W}$.

After $s(\cdot)$ [7], the representation at each position is a weighted sum of that of all pixels. With this adaptive mechanism, the feature representations at each position have stronger contextual relations with the same semantic class surroundings, and weaker with the different semantic class areas. The augmented feature has a global visual field, and could selectively aggregate pieces of information according to learned contextual relationships, thus meliorating intra-class consistency and inter-class separability.

2.3 Exterior Contextual-Relation Module

In a clinical setting, the doctor’s diagnosis of one lesion area is not isolated, but associates with previously seen circumstances. Based on this critical observation, region features belonging to the same semantic class of all training data should have contextual relations. Therefore, we propose a brand-new contextual relation exploring module across different samples.

Contextual region embedding. For a given feature $\mathbf{A} \in \mathbb{R}^{C \times H \times W}$, we first utilize a transformation function $\psi(\cdot)$, which is implemented by 1×1 conv \rightarrow BN \rightarrow ReLU, to compute a coarse segmentation map $\mathbf{M} \in \mathbb{R}^{1 \times H \times W}$, where each entry indicates the degree that the corresponding pixel belongs to the polyp region. Then the contextual region embedding is computed as below:

$$\mathbf{E} = \phi(\mathbf{M})^\top \cdot \phi(\mathbf{A}) \quad (1)$$

Here, $\phi(\cdot)$ is flatten function, and \cdot is matrix multiplication. $\mathbf{E} \in \mathbb{R}^C$.

Contextual relation matrix. Suppose that the buffered region embeddings are $\mathbb{E} = \{\mathbf{E}_1, \mathbf{E}_2, \dots, \mathbf{E}_S\} \in \mathbb{R}^{S \times C}$ where S is the bank size, and flattened feature representations of current mini-batch are $\mathbb{A} = \{\phi(\mathbf{A}_1), \phi(\mathbf{A}_2), \dots, \phi(\mathbf{A}_B)\}$ where B is the batchsize. Then we perform a matrix multiplication between them and apply a softmax layer to calculate the contextual attention map $\mathbb{X} \in \mathbb{R}^{HW \times B \times S}$:

$$x_{zji} = \frac{\exp(\mathbb{E}_i \cdot \mathbb{A}_{jz})}{\sum_{i=1}^N \exp(\mathbb{E}_i \cdot \mathbb{A}_{jz})} \quad (2)$$

where x_{zji} measures contextual relation in the z^{th} pixel between i^{th} image and j^{th} image. Note that the more similar feature representations of the two images contributes to greater correlation between them.

Augmented representations. The final augmented feature representations is computed by:

$$\mathbb{Y} = \rho(\delta(\mathbb{X} \cdot \mathbb{E})) \in \mathbb{R}^{B \times C \times H \times W} \quad (3)$$

where $\delta(\cdot)$ is the transpose function used to adjust the dimension order, and $\rho(\cdot)$ is the unflatten function used to recover spatial dimension.

2.4 Region Cross-Batch Memory

Inspired by non-parametric memory modules for embedding learning and contrastive learning [24,27,11,9,3], since we probe into the mutual contextual relations between different region embeddings across mini-batches, a memory concept is adopted and hence used to store previously seen embeddings. Furthermore, the work in [24] revealed “slow drift” phenomena which signify features drift exceptionally slow even as the model parameters are updating throughout the training process. The above discovery indicates the past mini-batches can be a considerably important resource, especially in medical computation. However, the embeddings too far away from the current mini-batch could cause feature-level inconsistency, which implies that the past entities should be iteratively discarded. Therefore, we operate the memory bank as a queue with a first-in-first-out principle.

Specifically, at the early stage of training, we initialize the memory by filling all the calculated contextual region embeddings. When the number of elements reaches the bank size S , we enqueue the region embeddings of the current mini-batch and dequeue the entities of the earliest mini-batch. Significantly, the setting of bank size S should be moderate: excessive small size could not arise rich contextual relations and excessive large size usually cause out-of-date data. The Region Cross-Batch Memory will be removed as inference, and the ECR will be employed to capture self-contextual relations as same as ICR.

2.5 Loss Functions

Similar to [5,30], we adopt the deep supervision strategy for three intermediate maps of decoder branch and coarse segmentation map M . And each is up-sampled to the same size as the label. For the loss function, we employ the combination of a weighted binary cross entropy (BCE) loss \mathcal{L}_{wbce} [25] and a Dice loss \mathcal{L}_{Dice} . In \mathcal{L}_{wbce} , each pixel will be assigned with a weight α . Hard pixel corresponds to larger α and simple pixel will be assigned a smaller one. The \mathcal{L}_{Dice} can better compare the structural similarities between prediction and Ground-Truth. Therefore, this strategy could consider both pixel-level and region-level measurement.

3 Experiments

3.1 Datasets

Experiments are conducted on three polyp segmentation datasets: EndoScene [22], Kvasir-SEG [17], and PICCOLO [19]. EndoScene contains 912 manually segmented White-Light images. We use the default split for training, validation, and testing. Kvasir-SEG contains 1000 White-Light images with pixel-level manual labels. We randomly choose 60% of the dataset as training set, 20% as validation set, and the remaining as test set. The last is the recently released PICCOLO

Table 1. Quantitative results on EndoScene.

Methods	MAE	Recall	Precision	Accuracy	Dice	IoU	\mathcal{F}	S_α
U-Net[18]	4.4	75.15	87.26	95.56	73.78	66.54	68.78	83.54
U-Net++[32]	4.5	73.27	88.58	95.49	72.88	64.58	63.68	82.41
ResUNet++[10]	6.3	50.72	79.39	93.71	52.41	44.33	43.60	71.02
PraNet[5]	3.5	82.56	90.52	96.61	81.73	74.38	75.79	88.00
ACSNet[30]	3.0	85.53	92.27	97.03	85.15	78.67	81.58	90.54
Ours	3.0	85.57	91.74	96.98	85.41	78.86	83.20	90.79

Table 2. Quantitative results on Kvasir-SEG.

Methods	MAE	Recall	Precision	Accuracy	Dice	IoU	\mathcal{F}	S_α
U-Net[18]	4.2	88.60	88.84	95.83	85.97	78.70	73.13	88.36
U-Net++[32]	5.2	88.04	85.93	94.84	84.16	76.02	70.33	87.17
ResUNet++[10]	5.6	85.58	83.52	94.35	81.09	72.73	64.75	85.22
PraNet[5]	3.1	90.45	92.55	96.94	89.20	83.61	77.97	90.96
ACSNet[30]	3.2	91.29	91.64	96.75	89.32	83.83	79.04	90.96
Ours	2.9	90.35	93.1	97.13	90.14	84.44	82.05	91.49

dataset, which contains 3433 manually annotated images (2131 White-Light images and 1302 Narrow-Band images). We use the default data splitting, which is 2203 images for the training set, 897 images for the validation set, and 333 images for the test set. All the images are resized to 224×224 in our experiments.

3.2 Implementation Details and Evaluation Metrics

Our model is implemented in Pytorch and trained on a single NVIDIA RTX 2080Ti. We utilize data augmentation strategies such as random horizontal and vertical flips, zoom, shift, and rotation. The memory bank size is set to 20 for Kvasir-SEG, and 40 for EndoScene and PICCOLO. We employ the Adam optimizer with a learning rate of $1e-4$ for 150 epochs. And the batch-size is set as 4 for all datasets.

Following [5,30], we use five metrics for quantitative evaluation, including ‘‘MAE’’, ‘‘Recall’’, ‘‘Precision’’, ‘‘Accuracy’’, ‘‘Dice’’, ‘‘Intersection-over-Union’’. Since the segmented boundary could help the doctor to get the information of polyp size, measuring the boundary quality is a critical angle in the experiment. Based on this, we further introduce a metric boundary F-measure \mathcal{F} [13] to measure the contour-based accuracy of the algorithm. S_α [4] is also adopted to evaluate the global structural similarities between prediction and Ground-Truth.

3.3 Results and Analysis

We compare our DCRNet with three medical image segmentation methods: U-Net[18], U-Net++[32], ResUNet++[10], and two SOTA polyp segmentation methods: PraNet[5] and ACSNet[30]. The segmentation results of PraNet[5] and ACSNet[30] are reproduced using the official released code with default settings.

Table 3. Quantitative results on PICCOLO.

Methods	MAE	Recall	Precision	Accuracy	Dice	IoU	\mathcal{F}	S_α
U-Net[18]	5.0	68.41	85.17	95.00	66.81	60.59	57.04	79.12
U-Net++[32]	5.4	70.07	83.93	94.64	68.21	61.48	58.11	79.07
ResUNet++[10]	5.8	61.05	85.75	94.18	60.24	53.68	47.04	75.15
PraNet[5]	3.0	76.57	90.95	97.02	75.34	69.77	65.88	84.71
ACSNet[30]	2.6	86.81	89.06	97.40	83.49	77.88	75.04	-
Ours	2.0	88.63	88.09	98.01	85.13	79.43	78.09	89.70

Table 4. Model and inference analysis on PICCOLO.

Methods	Inference(FPS)	Model size(MB)	Dice
PraNet	~24fps	30.5MB	75.34
ACSNet	~22fps	29.5MB	83.49
Ours	~53fps	28.7MB	85.13

Results on EndoScene. As shown in Table. 1, our DCRNet outperforms all SOTAs over most of metrics. With the improvement of *Dice*, *IoU* and S_α , our model achieves the better performance in the similarity of the overall region. And the great margin over \mathcal{F} suggests that our DCRNet is significantly more accurate for polyp boundary.

Results on Kvasir-SEG. The results are listed in Table. 2. Similarly, our model achieves the best performance and suppress others over most of metrics. And our method is the only one that can make *Dice* above 90, and can make MAE below 3. This boosted results further demonstrate the robustness and effectiveness of our DCRNet.

Results on PICCOLO. Since the PICCOLO[19] has the most data and the most complex scene in all publicly available benchmarks, the excellent performance on it could better report the robustness in clinical application. As shown in Table. 3, our DCRNet outperforms all SOTAs by a considerable margin in most of metrics, boosting *Dice* to 85.12, *IoU* to 79.31, \mathcal{F} to 77.88 and S_α to 89.70 respectively. Moreover, as shown in Figure. 2, our proposed DCRNet can consistently obtain greater segmentation maps under diverse clinical scenarios, such as blurred boundary, brightness change, enormous and tiny polyp. These suggest that our model has a strong learning ability and can better handle realistic colonoscopy images in clinical circumstances.

Inference and model analysis. In Table. 4, we evaluate the inference time and model parameters of DCRNet and other SOTA algorithms with the same batchsize of 4 and 1080Ti GPU platform. As shown, our method runs drastically faster than others, and owns the minimum number of parameters. This implies that our model is more appropriate for clinical applications.

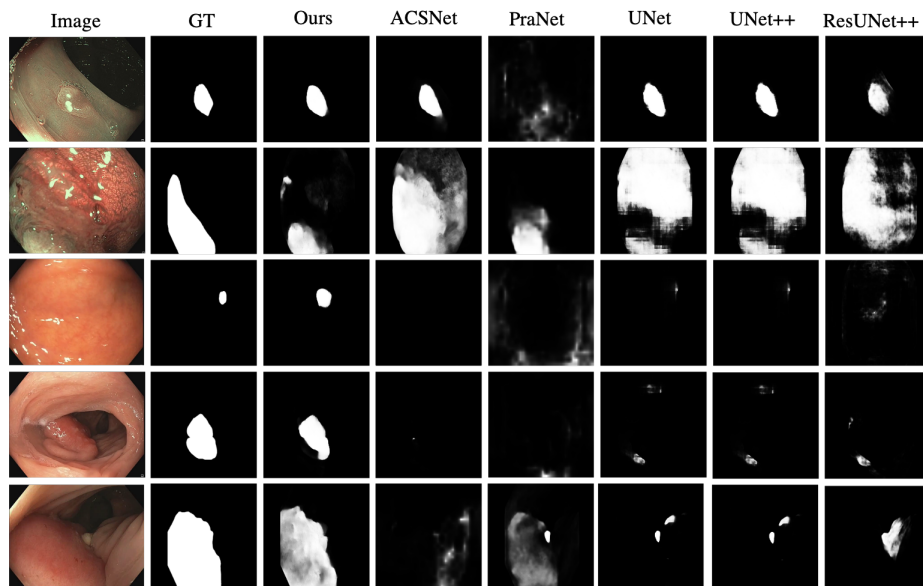


Fig. 2. Qualitative results of different methods on PICCOLO.

3.4 Ablation Study

To validate the effectiveness and necessity of each module in our proposed method, we compare DCRNet with its three variants in Table. 5. Specifically, the Backbone refers to the original U-Net with pretrained ResNet-34 encoder, and we successively add ICR, ECR, and ROM to it. As shown, with the progressive introduction of ICR, ECR, and ROM, our algorithm has witnessed a certain degree of performance improvement, boosting Dice by 0.68%, 1.11%, 2.31% respectively. It is noteworthy that the improvement brought by Backbone + ECR + ROM on PICCOLO is more remarkable than that on EndoScene. This observation indicates that simulating such cross-image clinical diagnosis is momentous for polyp segmentation tasks, and confirms the effectiveness and importance of our core idea.

4 Conclusion

In this paper, we propose Duplex Contextual Relation Network (DCRNet) for polyp segmentation. The proposed network contains two parallel modules: *Interior Contextual-Relation Module* and *Exterior Contextual-Relation Module* which are utilized to capture within-image and cross-image contextual relations respectively. To store the characteristic region embedding from all the images, a memory bank is designed for ECR and operates as a queue. Experimental results

Table 5. Ablation Study for DCRNet on EndoScene and PICCOLO datasets.

Settings	EndoScene			PICCOLO		
	Dice	IoU	MAE	Dice	IoU	MAE
Backbone	81.48	74.26	3.5	78.59	72.65	3.3
Backbone + ICR	85.23	78.88	3.0	79.27	73.38	3.8
Backbone + ECR	83.61	76.69	3.2	79.7	74.12	3.1
Backbone + ECR + ROM	84.93	78.31	3.0	82.01	76.22	3
Backbone + ICR + ECR + ROM	85.41	78.86	3.0	85.12	79.31	2.0

show that the proposed DCRNet achieves the state-of-the-art performance on three datasets in terms of the widely-used evaluation metrics. Ablation studies are conducted to demonstrate the effectiveness of each proposed component.

References

1. Akbari, M., Mohrekeesh, M., Nasr-Esfahani, E., Soroushmehr, S.R., Karimi, N., Samavi, S., Najarian, K.: Polyp segmentation in colonoscopy images using fully convolutional network. In: 2018 40th Annual International Conference of the IEEE Engineering in Medicine and Biology Society (EMBC). pp. 69–72. IEEE (2018)
2. Brandao, P., Mazomenos, E., Ciuti, G., Calì, R., Bianchi, F., Menciassi, A., Dario, P., Koulaouzidis, A., Arezzo, A., Stoyanov, D.: Fully convolutional neural networks for polyp segmentation in colonoscopy. In: Medical Imaging 2017: Computer-Aided Diagnosis. vol. 10134, p. 101340F. International Society for Optics and Photonics (2017)
3. Chen, X., Fan, H., Girshick, R., He, K.: Improved baselines with momentum contrastive learning. arXiv preprint arXiv:2003.04297 (2020)
4. Fan, D.P., Cheng, M.M., Liu, Y., Li, T., Borji, A.: Structure-measure: A new way to evaluate foreground maps. In: Proceedings of the IEEE international conference on computer vision. pp. 4548–4557 (2017)
5. Fan, D.P., Ji, G.P., Zhou, T., Chen, G., Fu, H., Shen, J., Shao, L.: Pranel: Parallel reverse attention network for polyp segmentation. In: International Conference on Medical Image Computing and Computer-Assisted Intervention. pp. 263–273. Springer (2020)
6. Fang, Y., Chen, C., Yuan, Y., Tong, K.y.: Selective feature aggregation network with area-boundary constraints for polyp segmentation. In: International Conference on Medical Image Computing and Computer-Assisted Intervention. pp. 302–310. Springer (2019)
7. Fu, J., Liu, J., Tian, H., Li, Y., Bao, Y., Fang, Z., Lu, H.: Dual attention network for scene segmentation. In: Proceedings of the IEEE/CVF Conference on Computer Vision and Pattern Recognition. pp. 3146–3154 (2019)
8. Gutmann, M., Hyvärinen, A.: Noise-contrastive estimation: A new estimation principle for unnormalized statistical models. In: Proceedings of the Thirteenth International Conference on Artificial Intelligence and Statistics. pp. 297–304. JMLR Workshop and Conference Proceedings (2010)
9. He, K., Fan, H., Wu, Y., Xie, S., Girshick, R.: Momentum contrast for unsupervised visual representation learning. In: Proceedings of the IEEE/CVF Conference on Computer Vision and Pattern Recognition. pp. 9729–9738 (2020)

10. Jha, D., Smedsrud, P.H., Riegler, M.A., Johansen, D., De Lange, T., Halvorsen, P., Johansen, H.D.: Resunet++: An advanced architecture for medical image segmentation. In: 2019 IEEE International Symposium on Multimedia (ISM). pp. 225–2255. IEEE (2019)
11. Li, S., Chen, D., Liu, B., Yu, N., Zhao, R.: Memory-based neighbourhood embedding for visual recognition. In: Proceedings of the IEEE/CVF International Conference on Computer Vision. pp. 6102–6111 (2019)
12. Mamonov, A.V., Figueiredo, I.N., Figueiredo, P.N., Tsai, Y.H.R.: Automated polyp detection in colon capsule endoscopy. *IEEE transactions on medical imaging* **33**(7), 1488–1502 (2014)
13. Martin, D.R., Fowlkes, C.C., Malik, J.: Learning to detect natural image boundaries using local brightness, color, and texture cues. *IEEE transactions on pattern analysis and machine intelligence* **26**(5), 530–549 (2004)
14. Mirasadi, M.S., Foruzan, A.H.: Content-based medical image retrieval of ct images of liver lesions using manifold learning. *International Journal of Multimedia Information Retrieval* **8**(4), 233–240 (2019)
15. Murugesan, B., Sarveswaran, K., Shankaranarayana, S.M., Ram, K., Joseph, J., Sivaprakasam, M.: Psi-net: Shape and boundary aware joint multi-task deep network for medical image segmentation. In: 2019 41st Annual International Conference of the IEEE Engineering in Medicine and Biology Society (EMBC). pp. 7223–7226. IEEE (2019)
16. Oord, A.v.d., Li, Y., Vinyals, O.: Representation learning with contrastive predictive coding. *arXiv preprint arXiv:1807.03748* (2018)
17. Pogorelov, K., Randel, K.R., Griwodz, C., Eskeland, S.L., de Lange, T., Johansen, D., Spampinato, C., Dang-Nguyen, D.T., Lux, M., Schmidt, P.T., et al.: Kvasir: A multi-class image dataset for computer aided gastrointestinal disease detection. In: Proceedings of the 8th ACM on Multimedia Systems Conference. pp. 164–169 (2017)
18. Ronneberger, O., Fischer, P., Brox, T.: U-net: Convolutional networks for biomedical image segmentation. In: International Conference on Medical image computing and computer-assisted intervention. pp. 234–241. Springer (2015)
19. Sánchez-Peralta, L.F., Pagador, J.B., Picón, A., Calderón, Á.J., Polo, F., Andraka, N., Bilbao, R., Glover, B., Saratzaga, C.L., Sánchez-Margallo, F.M.: Piccolo white-light and narrow-band imaging colonoscopic dataset: A performance comparative of models and datasets. *Applied Sciences* **10**(23), 8501 (2020)
20. Siegel, R.L., Miller, K.D., Goding Sauer, A., Fedewa, S.A., Butterly, L.F., Anderson, J.C., Cercek, A., Smith, R.A., Jemal, A.: Colorectal cancer statistics, 2020. *CA: a cancer journal for clinicians* **70**(3), 145–164 (2020)
21. Tajbakhsh, N., Gurudu, S.R., Liang, J.: Automated polyp detection in colonoscopy videos using shape and context information. *IEEE transactions on medical imaging* **35**(2), 630–644 (2015)
22. Vázquez, D., Bernal, J., Sánchez, F.J., Fernández-Esparrach, G., López, A.M., Romero, A., Drozdal, M., Courville, A.: A benchmark for endoluminal scene segmentation of colonoscopy images. *Journal of healthcare engineering* **2017** (2017)
23. Wang, W., Zhou, T., Yu, F., Dai, J., Konukoglu, E., Van Gool, L.: Exploring cross-image pixel contrast for semantic segmentation. *arXiv preprint arXiv:2101.11939* (2021)
24. Wang, X., Zhang, H., Huang, W., Scott, M.R.: Cross-batch memory for embedding learning. In: Proceedings of the IEEE/CVF Conference on Computer Vision and Pattern Recognition. pp. 6388–6397 (2020)

25. Wei, J., Wang, S., Huang, Q.: F³net: Fusion, feedback and focus for salient object detection. In: Proceedings of the AAAI Conference on Artificial Intelligence. vol. 34, pp. 12321–12328 (2020)
26. Wickstrøm, K., Kampffmeyer, M., Jenssen, R.: Uncertainty and interpretability in convolutional neural networks for semantic segmentation of colorectal polyps. *Medical image analysis* **60**, 101619 (2020)
27. Wu, Z., Xiong, Y., Yu, S.X., Lin, D.: Unsupervised feature learning via non-parametric instance discrimination. In: Proceedings of the IEEE Conference on Computer Vision and Pattern Recognition. pp. 3733–3742 (2018)
28. Yu, L., Chen, H., Dou, Q., Qin, J., Heng, P.A.: Integrating online and offline three-dimensional deep learning for automated polyp detection in colonoscopy videos. *IEEE journal of biomedical and health informatics* **21**(1), 65–75 (2016)
29. Yuan, Y., Chen, X., Wang, J.: Object-contextual representations for semantic segmentation. arXiv preprint arXiv:1909.11065 (2019)
30. Zhang, R., Li, G., Li, Z., Cui, S., Qian, D., Yu, Y.: Adaptive context selection for polyp segmentation. In: International Conference on Medical Image Computing and Computer-Assisted Intervention. pp. 253–262. Springer (2020)
31. Zhang, R., Zheng, Y., Poon, C.C., Shen, D., Lau, J.Y.: Polyp detection during colonoscopy using a regression-based convolutional neural network with a tracker. *Pattern recognition* **83**, 209–219 (2018)
32. Zhou, Z., Siddiquee, M.M.R., Tajbakhsh, N., Liang, J.: Unet++: A nested u-net architecture for medical image segmentation. In: Deep learning in medical image analysis and multimodal learning for clinical decision support, pp. 3–11. Springer (2018)